Power transmission coefficients for multi-step index optical fibres

Gotzon Aldabaldetreku, Joseba Zubia, Gaizka Durana, and Jon Arrue

University of the Basque Country,
Alda. Urquijo s/n, E-48013 Bilbao, Spain
gotzon.aldabaldetreku@ehu.es

Abstract: The aim of the present paper is to provide a single analytical expression of the power transmission coefficient for leaky rays in multi-step index (MSI) fibres. This expression is valid for all tunnelling and refracting rays and allows us to evaluate numerically the power attenuation along an MSI fibre of an arbitrary number of layers. We validate our analysis by comparing the results obtained for limit cases of MSI fibres with those corresponding to step-index (SI) and graded-index (GI) fibres. We also make a similar comparison between this theoretical expression and the use of the WKB solutions of the scalar wave equation.

OCIS codes: (060.0060) Fiber optics and optical communications; (060.2270) Fiber characterization; (060.2310) Fiber optics; (260.0260) Physical optics; (260.6970) Total internal reflection.

References and links

1. V. Levin, T. Baskakova, Z. Lavrova, A. Zubkov, H. Poisel, and K. Klein, "Production of multilayer polymer optical fibers," in *Proceedings of the eighth international conference on plastic optical fibers and applications-POF'99*, pp. 98–101 (Chiba (Japan), 1999).
2. K. Irie, Y. Uozu, and T. Yoshimura, "Structure design and analysis of broadband POF," in *Proceedings of the tenth international conference on plastic optical fibers and applications-POF'01*, pp. 73–79 (Amsterdam (The Netherlands), 2001).
3. J. Zubia, G. Aldabaldetreku, G. Durana, J. Arrue, H. Poisel, and C. A. Bunge, "Geometric optics analysis of multi-step index optical fibers," Fiber Integr. Opt. **23**, 121–156 (2004).
4. A. W. Snyder and J. D. Love, *Optical waveguide theory* (Chapman and Hall, London, 1983).
5. R. Sammut and A. W. Snyder, "Leaky modes on circular optical waveguides," Appl. Opt. **15**, 477–482 (1976).
6. A. W. Snyder and J. D. Love, "Tunnelling leaky modes on optical waveguides," Opt. Commun. **12**, 326–328 (1974).
7. J. D. Love and C. Winkler, "Attenuation and tunneling coefficients for leaky rays in multilayered optical waveguides," J. Opt. Soc. Am. **67**, 1627–1632 (1977).
8. J. D. Love and C. Winkler, "Refracting leaky rays in graded-index fibers," Appl. Opt. **17**, 2205–2208 (1978).
9. J. D. Love and C. Winkler, "A universal tunnelling coefficient for step- and graded-index multimode fibres," Opt. Quantum Electron. **10**, 341–351 (1978).
10. D. Gloge and E. A. J. Marcatili, "Multimode theory of graded-core fibers," Bell Syst. Tech. J. **52**, 1563–1578 (1973).
11. A. Ankiewicz, "Geometric optics theory of graded index optical fibres," Ph.D. thesis, Australian National University (1978).
12. D. Marcuse, D. Gloge, and E. A. J. Marcatili, "Guiding properties of fibers," in *Optical fiber telecommunications*, S. E. Miller and A. G. Chynoweth, eds., chap. 3 (Academic Press, Inc., San Diego, California, 1979).
13. S. Zhu, A. W. Yu, D. Hawley, and R. Roy, "Frustrated total internal reflection: A demonstration and review," Am. J. Phys. **54**, 601–606 (1986).
14. F. P. Zanella, D. V. Magalhães, M. M. Oliveira, R. F. Bianchi, L. Misoguti, and C. R. Mendonça, "Frustrated total internal reflection: A simple application and demonstration," Am. J. Phys. **71**, 494–496 (2003).
15. A. A. Stahlhofen, "Comment on "Frustrated total internal reflection: A simple application and demonstration," F. P. Zanella *et al.* [Am. J. Phys. 71 (5), 494–496 (2003)]," Am. J. Phys. **72**, 412 (2004).

#10272 - $15.00 USD Received 11 January 2006; revised 6 February 2006; accepted 13 February 2006

16. O. Bryngdahl, "Evanescent waves in optical imaging," in *Progress in optics XI*, E. Wolf, ed., chap. 4 (North-Holland, Amsterdam, 1973).
17. R. J. Black and A. Ankiewicz, "Fiber-optic analogies with mechanics," Am. J. Phys. **53**, 554–563 (1985).
18. A. W. Snyder, D. J. Mitchell, and C. Pask, "Failure of geometric optics for analysis of circular optical fibers," J. Opt. Soc. Am. **64**, 608–614 (1974).
19. A. W. Snyder and D. J. Mitchell, "Leaky rays on circular optical fibers," J. Opt. Soc. Am. **64**, 599–607 (1974).
20. A. W. Snyder and D. J. Mitchell, "Generalized Fresnel's laws for determining radiation loss from optical waveguides and curved dielectric structures," Optik **40**, 438–459 (1974).
21. A. W. Snyder and J. D. Love, "Reflection at a curved dielectric interface – Electromagnetic tunneling," IEEE Trans. Microwave Theory Tech. **23**, 134–141 (1975).
22. J. D. Love and C. Winkler, "Generalized Fresnel power transmission coefficients for curved graded-index media," IEEE Trans. Microwave Theory Tech. **28**, 689–695 (1980).
23. M. Abramowitz and I. A. Stegun, *Handbook of mathematical functions with formulas, graphs, and mathematical tables* (Dover Publications, Inc., New York, 1965).
24. J. D. Love and C. Winkler, "The step index limit of power law refractive index profiles for optical waveguides," J. Opt. Soc. Am. **68**, 1188–1191 (1978).
25. M. Born and E. Wolf, *Principles of optics*, 6th ed. (Pergamon Press, New York, 1990).
26. Mitsubishi Rayon Co., Ltd.: "Eska-Miu," URL http://www.pofeska.com.
27. D. Marcuse, *Principles of optical fiber measurements*, chap. 4 (Academic Press, Inc., London, 1981).
28. Japanese Standards Association, "Test methods for structural parameters of all plastic multimode optical fibers," Tech. Rep. JIS C 6862, JIS, Tokyo, Japan (1990).
29. A. Ankiewicz and C. Pask, "Tunnelling rays in graded-index fibres," Opt. Quantum Electron. **10**, 83–93 (1978).

1. Introduction

Multimode optical waveguides of circular cross-section, such as multi-step index (MSI) fibres, can propagate leaky rays in addition to bound rays, when they are illuminated by sources which emit light over a wide range of directions, as is the case of light emitting diodes (LEDs) [1–5]. These leaky rays are responsible for the loss of power by radiation and, therefore, they have a great significance in the description of light propagation within a multimode optical fibre.

After a sufficiently long fibre distance from the source, practically all leaky ray power has radiated away, whereas bound rays convey nearly all of the remaining power within the fibre. Once we reach this steady state, light propagation can be entirely described by bound rays alone. Nevertheless, in the intermediate region both bound and leaky rays are necessary to provide an accurate description of light propagation, since the latter can contribute significantly to the total light power.

It is important to keep in mind that this intermediate region or transient state can extend as far as several kilometres. For this reason, and also taking into account that the usual range of MSI polymer optical fibres (MSI-POFs) rarely goes beyond 100 metres [2], in nearly all cases it is crucial that we assess accurately the power radiated by leaky rays, since they could modify the transmission properties of these fibres. These modifications could, in turn, have an effect on the bandwidth or on some other parameters that determine the fibre performance.

Leaky rays can be classified into two subclasses as well: refracting and tunnelling rays [6]. Tunnelling rays undergo a very slow leakage compared to refracting rays and, therefore, they play a major role in the determination of the power attenuation along a fibre [7]. Nevertheless, the evaluation of the power attenuation by an electromagnetic-mode analysis presents a boundary-value problem that is virtually intractable for geometries involving more than two layers [7], which is the usual case in MSI fibres.

We can overcome such a problem if we linearize the square of the core refractive index in the profile of the MSI fibre [8]. Then, we can make use of a single analytical expression based on the method of uniform approximation and valid for all leaky rays. Such an expression has been previously derived in Ref. [9] for step-index (SI) and graded-index (GI) fibres, although it must be stressed that there are many typographical errors that invalidate its use, unless they are corrected. It is our purpose to recalculate this expression and make it suitable for MSI fibres.

#10272 - $15.00 USD Received 11 January 2006; revised 6 February 2006; accepted 13 February 2006

Once recalculated, its implementation in computational models that use the ray-tracing method will allow obtaining much more accurate and realistic simulation results.

The structure of the paper is as follows. We begin in section 2 with a brief review of the classification of rays into bound, tunnelling and refracting rays and explain the physical mechanism that gives rise to the existence of tunnelling rays. Then, we give the mathematical derivation of the power transmission coefficient for MSI fibres by using the method of uniform approximation. We also provide the suitable expressions based on the WKB solutions and restrict their applicability to regions away from the boundary between tunnelling and refracting rays. Afterwards, we carry out several calculations for different types of MSI fibres and discuss the results obtained. Finally, we summarize the main conclusions.

2. Theoretical analysis

2.1. Classification of rays in MSI fibres

The most significant characteristic of MSI fibres that differentiates them from their SI or GI counterparts is their multilayered core. The most general refractive index profile in MSI fibres can be expressed as

$$n(r) = \begin{cases} n_1; & r < \rho_1, \\ n_2; & \rho_1 \leqslant r < \rho_2, \\ \quad \vdots & \\ n_N; & \rho_{N-1} \leqslant r < \rho_N, \\ n_{cl}; & r \geqslant \rho_N, \end{cases} \tag{1}$$

where we assume, for the sake of simplicity, that the cladding extends to infinity.

A convenient way to classify rays in MSI fibres is to make use of the ray path equation $g(r)$ to determine the range of values of the radial coordinate r for which rays can propagate. It is defined as [3]

$$g(r) = n^2(r) - \tilde{\beta}^2 - \frac{\tilde{l}^2 \rho_N^2}{r^2}, \tag{2}$$

where the ray invariants $\tilde{\beta}$ and $\tilde{l}$ define the ray path

$$\begin{aligned} &\tilde{\beta} = n_i \cos\theta_{z_i}; \\ &\tilde{l} = \frac{\rho_i}{\rho_N} n_i \sin\theta_{z_i} \cos\theta_{\phi_i}; \end{aligned} \qquad i = 1 \ldots N, \tag{3}$$

θ_{z_i} being the angle between the ray path and the longitudinal axis and θ_{ϕ_i} the angle between the ray path projection onto the fibre cross-section and the azimuthal direction, both measured at a certain *i*th layer.

Ray paths can exist only if the right-side of Eq. (2) is non-negative, corresponding to an oscillating field, whereas we have an evanescent field if the right-side of Eq. (2) is negative [4, 10–12]. To be trapped within an MSI fibre of outermost radius ρ_N, a ray must have $g(r)|_{r=\rho_N^+} < 0$, i.e.

$$n_{cl}^2 - \tilde{\beta}^2 - \tilde{l}^2 < 0. \tag{4}$$

Taking this into account, we can classify rays as follows:

- *Bound rays:* These rays are bound to the fibre core and do not leak into the cladding. $g(r) < 0 \quad \forall r > \rho_N$.

$$\text{Bound rays} \quad \begin{cases} n_{cl} \leqslant \tilde{\beta} \leqslant n_1, \\ 0 \leqslant \tilde{l} \leqslant \tilde{l}_{max}\left(\tilde{\beta}\right). \end{cases} \tag{5}$$

#10272 - $15.00 USD Received 11 January 2006; revised 6 February 2006; accepted 13 February 2006

- *Tunnelling rays:* These rays satisfy the two conditions $\tilde{\beta}^2 < n_{cl}^2$ and $\tilde{\beta}^2 + \tilde{l}^2 \geqslant n_{cl}^2$.

$$\text{Tunnelling rays} \quad \begin{cases} 0 \leqslant \tilde{\beta} < n_{cl}, \\ \left(n_{cl}^2 - \tilde{\beta}^2\right)^{1/2} \leqslant \tilde{l} \leqslant \tilde{l}_{max}\left(\tilde{\beta}\right). \end{cases} \tag{6}$$

- *Refracting rays:* These rays reach the core-cladding interface. $g(r)|_{r=\rho_N^+} > 0$, that is, $0 \leqslant \tilde{\beta}^2 + \tilde{l}^2 < n_{cl}^2$.

In the statements above, $\tilde{l}_{max}\left(\tilde{\beta}\right)$ is the maximum value of $\tilde{l}$ along the curve $g(r) = 0$, i.e.

$$\tilde{l}_{max}^2\left(\tilde{\beta}\right) = \left(n_x^2 - \tilde{\beta}^2\right)\frac{\rho_x^2}{\rho_N^2}, \tag{7}$$

x being an integer value satisfying

$$x = \min\{\text{all possible values of } i\} \quad \text{so that} \quad \tilde{\beta} \geqslant \tilde{\beta}_{min}; \qquad i = 1 \ldots N,$$

and

$$\tilde{\beta}_{min}^2 = \begin{cases} \max\left\{0, \dfrac{\rho_{j+1}^2 n_{j+1}^2 - \rho_i^2 n_i^2}{\rho_{j+1}^2 - \rho_i^2}\right\}; & \begin{cases} i = 1 \ldots N-1, \\ j = i \ldots N-1, \end{cases} \\ 0; & i = N. \end{cases} \tag{8}$$

2.2. Tunnelling rays in MSI fibres

Rays that are tunnelling are neither bound nor refracting and satisfy the conditions shown above. These rays disappear in the core at the turning points and reappear in the cladding at a finite distance from the core-cladding interface. For these rays to be able to propagate in the cladding, it is necessary to have a positive $g(r)$ for all values of r beyond a certain radius r_{rad} given by the condition $g(r)|_{r=r_{rad}} = 0$. Hence

$$r_{rad} = \frac{\tilde{l}\rho_N}{\left(n_{cl}^2 - \tilde{\beta}^2\right)^{1/2}}. \tag{9}$$

At each turning point, part of the ray power is lost to the cladding by means of a tunnelling mechanism, analogous to the frustrated total internal reflection [13–17], caused in this instance by the curvature of the core-cladding interface [6]. The ray theory does not serve to understand the origin of the physical mechanism that produces this type of radiation [18]. Its explanation has to be looked for by using Maxwell's equations and, more specifically, the modal solution of the wave equation [5, 19].

Nevertheless, we can still retain the ray paths of geometric optics and incorporate this wave effect by conveniently defining a power transmission coefficient T and assuming that power loss occurs only at turning points along the ray path [4]. Furthermore, such an approach has the additional advantage of allowing us to extend its applicability to the analysis of refracting rays. Therefore, we define T as the fraction of incident power transmitted to the cladding

$$T = 1 - \frac{\text{power of the reflected ray}}{\text{power of the incident ray}}. \tag{10}$$

From a knowledge of the power transmission coefficient, we can define the power attenuation coefficient γ of a ray as [7, 20]

$$\gamma = T/z_p, \tag{11}$$

#10272 - $15.00 USD Received 11 January 2006; revised 6 February 2006; accepted 13 February 2006

where z_p, or ray half-period, is the axial distance between successive turning points at which power is lost [3]. Assuming that γ is constant, the ray power $P(z)$ at a distance z along the fibre attenuates according to

$$P(z) = P(0)\exp(-\gamma z). \tag{12}$$

2.3. *Mathematical derivation of the power transmission coefficient*

The derivation of the power transmission coefficient relies on the linearization of the square of the core refractive index of the MSI fibre at the top of the jump at $r = \rho_N$, as shown in Fig. 1 [7, 8]. We obtain

$$n^2(r) = \begin{cases} \delta(r-\rho_N) + n_N^2; & r \lesssim \rho_N, \\ n_{cl}^2; & r \gtrsim \rho_N, \end{cases} \tag{13}$$

where n_N is the refractive index and ρ_N is the outer radius of the Nth layer (i.e. the outermost one).

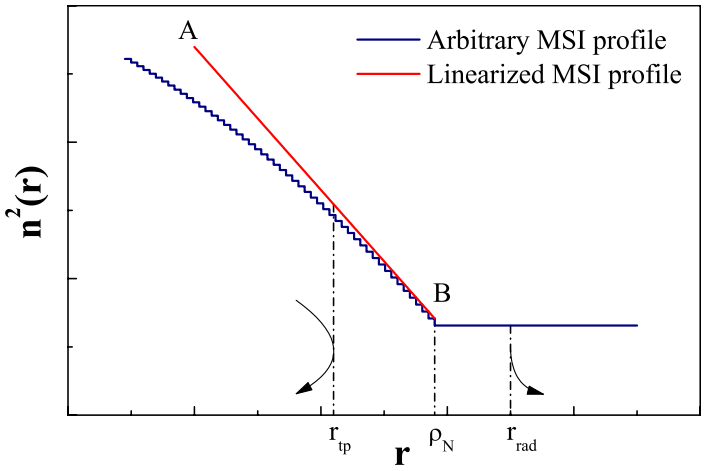

Fig. 1. The linearized profile used in the analysis corresponds to $\overline{AB}$ (red line). At r_{tp} the ray is partially reflected and the position r_{rad} in the cladding stands for the point where the transmitted ray reappears.

The value of δ is the slope of the core profile at $r = \rho_N^-$

$$\delta = \left.\frac{\mathrm{d}n^2(r)}{\mathrm{d}r}\right|_{r=\rho_N^-} = \frac{n_N^2 - n_{N-1}^2}{\rho_N - \rho_{N-1}}, \tag{14}$$

and always $\delta < 0$ whenever the refractive index profile decreases with r.

Provided that the change in the refractive index profile over this region is small, i.e. that we are considering weakly guiding fibres, the results obtained are independent of polarization [20]. By assuming that $k\rho_N \gg 1$, so that the fields exhibit local-plane-wave, or ray, characteristics [21, 22], we can work with the solutions of the scalar wave equation. ($k = 2\pi/\lambda$ is the wavenumber and λ the wavelength in vacuum.)

The linearization of $n^2(r)$ in Eq. (13) allows us to calculate these solutions by following the same procedure as for GI fibres, which was accurately described in Ref. [9]. Nevertheless, it is worthy of remark that there are many typographical errors in this reference which are very

#10272 - $15.00 USD Received 11 January 2006; revised 6 February 2006; accepted 13 February 2006

difficult to track down. Furthermore, in many cases they cannot be easily corrected, unless the stated problem is solved from the beginning. Consequently, and for the sake of completeness, we have decided to include the detailed mathematical derivation, indicating the exact location of such mistakes and providing the correct expressions, where appropriate.

Using the ray invariants defined in subsection 2.1, the solutions of the scalar wave equation in cylindrical coordinates (r,ϕ,z) are of the form $\Psi(r)\exp\left[\imath k\left(\tilde{\beta}z+\rho_N\tilde{l}\phi\right)\right]$, where $\Psi(r)$ satisfies [8]

$$\frac{\mathrm{d}^2\Psi}{\mathrm{d}r^2}+\frac{1}{r}\frac{\mathrm{d}\Psi}{\mathrm{d}r}+k_r^2(r)\Psi=0, \tag{15}$$

and $k_r(r)$ is the radial component of the local plane wave vector

$$k_r(r)=k\left[n^2(r)-\tilde{\beta}^2-\frac{\tilde{l}^2\rho_N^2}{r^2}\right]^{1/2}. \tag{16}$$

Using the transformation $\Psi(r)=\Phi(r)/\sqrt{r}$, Eq. (15) reduces to

$$\frac{\mathrm{d}^2\Phi}{\mathrm{d}r^2}+k^2\left[n^2(r)-\tilde{\beta}^2-\left(\tilde{l}^2-\frac{1}{4k^2\rho_N^2}\right)\frac{\rho_N^2}{r^2}\right]\Phi=0, \tag{17}$$

and the term $1/\left(4k^2\rho_N^2\right)$ can be safely neglected compared with $\tilde{l}^2$. Therefore,

$$\frac{\mathrm{d}^2\Phi}{\mathrm{d}r^2}+k_r^2(r)\Phi=0. \tag{18}$$

After a change of variables this leads to the Airy equation [23]

$$\frac{\mathrm{d}^2\Phi}{\mathrm{d}\xi^2}-\xi\Phi=0, \tag{19}$$

whose solutions are in terms of the Airy functions [9]

$$\Phi=C\left[\frac{-\xi(r)}{k_r^2(r)}\right]^{1/4}\left[\mathrm{Ai}(\xi(r))\pm\imath\mathrm{Bi}(\xi(r))\right], \tag{20}$$

where C is a constant and

$$\xi(r)=\begin{cases}-\left[\dfrac{3}{2}\displaystyle\int^r k_r(r)\,\mathrm{d}r\right]^{2/3}; & k_r^2(r)>0,\\ +\left[\dfrac{3}{2}\displaystyle\int^r |k_r(r)|\,\mathrm{d}r\right]^{2/3}; & k_r^2(r)<0.\end{cases} \tag{21}$$

(Please note that the absolute value of Eq. (23) of Ref. [9] was inappropriately placed.)

These solutions can be thought of as connecting expressions between the oscillatory behaviour when $-\xi\gg1$ and the exponential behaviour when $\xi\gg1$. Let us now separate Eq. (21) into

$$\xi_1(r)=\begin{cases}-\left[\dfrac{3}{2}\displaystyle\int_r^{r_{tp}} k_{r_1}(r)\,\mathrm{d}r\right]^{2/3}; & k_{r_1}^2(r)>0\\ +\left[\dfrac{3}{2}\displaystyle\int_{r_{tp}}^r |k_{r_1}(r)|\,\mathrm{d}r\right]^{2/3}; & k_{r_1}^2(r)<0\end{cases} \qquad \text{if} \quad r\lesssim\rho_N, \tag{22}$$

$$\xi_2(r)=\begin{cases}-\left[\dfrac{3}{2}\displaystyle\int_{r_{rad}}^r k_{r_2}(r)\,\mathrm{d}r\right]^{2/3}; & k_{r_2}^2(r)>0\\ +\left[\dfrac{3}{2}\displaystyle\int_r^{r_{rad}} |k_{r_2}(r)|\,\mathrm{d}r\right]^{2/3}; & k_{r_2}^2(r)<0\end{cases} \qquad \text{if} \quad r\gtrsim\rho_N, \tag{23}$$

#10272 - $15.00 USD Received 11 January 2006; revised 6 February 2006; accepted 13 February 2006

where

$$k_{r_1}(r)=\begin{cases} k\left[n^2(r)-\tilde{\beta}^2-\dfrac{\tilde{l}^2\rho_N^2}{r^2}\right]^{1/2}; & n^2(r)>\tilde{\beta}^2+\dfrac{\tilde{l}^2\rho_N^2}{r^2} \\ \imath k\left[\tilde{\beta}^2+\dfrac{\tilde{l}^2\rho_N^2}{r^2}-n^2(r)\right]^{1/2}; & n^2(r)<\tilde{\beta}^2+\dfrac{\tilde{l}^2\rho_N^2}{r^2} \end{cases} \quad \text{if} \quad r\lesssim\rho_N, \tag{24}$$

$$k_{r_2}(r)=\begin{cases} k\left(n_{cl}^2-\tilde{\beta}^2-\dfrac{\tilde{l}^2\rho_N^2}{r^2}\right)^{1/2}; & n_{cl}^2>\tilde{\beta}^2+\dfrac{\tilde{l}^2\rho_N^2}{r^2} \\ \imath k\left(\tilde{\beta}^2+\dfrac{\tilde{l}^2\rho_N^2}{r^2}-n_{cl}^2\right)^{1/2}; & n_{cl}^2<\tilde{\beta}^2+\dfrac{\tilde{l}^2\rho_N^2}{r^2} \end{cases} \quad \text{if} \quad r\gtrsim\rho_N. \tag{25}$$

In the equations above r_{tp} and r_{rad} are the roots of $k_{r_1}(r)=0$ and $k_{r_2}(r)=0$, respectively [4]. In the latter case it is straightforward to show that r_{rad} corresponds to Eq. (9), whereas in the former case the equation to solve is

$$ar^3+br^2+c=0,$$

where

$$\begin{aligned} a&=\delta, \\ b&=-\delta\rho_N+n_N^2-\tilde{\beta}^2, \\ c&=-\tilde{l}^2\rho_N^2, \end{aligned}$$

and they always satisfy $a<0$, $b>0$ and $c<0$ provided that $\tilde{\beta}<n_{cl}$ and the refractive index profile decreases with r. Under such conditions, and out of the three possible solutions, r_{tp} corresponds to

$$r_{tp}=-\frac{1}{3a}\left[b+\frac{1}{2^{1/3}}\left(L+\sqrt{3}M\right)\right], \tag{26}$$

where

$$\begin{aligned} L&=\left(F^2+G^2\right)^{1/6}\cos\left[\frac{1}{3}\arctan\left(\frac{G}{F}\right)\right], \\ M&=\left(F^2+G^2\right)^{1/6}\sin\left[\frac{1}{3}\arctan\left(\frac{G}{F}\right)\right], \end{aligned}$$

and

$$\begin{aligned} F&=-2b^3-27a^2c, \\ G&=3\sqrt{3}\left(-4a^2b^3c-27a^4c^2\right)^{1/2}. \end{aligned}$$

The asymptotic expansions of the Airy functions must represent the fields of [4]

(i) the incident ray approaching the turning point r_{tp} and the reflected ray leaving r_{tp} (both for $r\lesssim\rho_N$), and

(ii) the transmitted ray leaving the radiation caustic r_{rad} (for $r\gtrsim\rho_N$).

#10272 - $15.00 USD Received 11 January 2006; revised 6 February 2006; accepted 13 February 2006

Thus, we set (compare the set of equations below with Eq. (24) of Ref. [9])

$$\Phi^i(r) = A\left[\frac{-\xi_1(r)}{k_{r_1}^2(r)}\right]^{1/4}\left[\mathrm{Ai}(\xi_1(r)) + \imath\mathrm{Bi}(\xi_1(r))\right], \tag{27}$$

$$\Phi^r(r) = R\left[\frac{-\xi_1(r)}{k_{r_1}^2(r)}\right]^{1/4}\left[\mathrm{Ai}(\xi_1(r)) - \imath\mathrm{Bi}(\xi_1(r))\right], \tag{28}$$

$$\Phi^t(r) = S\left[\frac{-\xi_2(r)}{k_{r_2}^2(r)}\right]^{1/4}\left[\mathrm{Ai}(\xi_2(r)) - \imath\mathrm{Bi}(\xi_2(r))\right], \tag{29}$$

where A, R and S are constants related to the amplitudes of the corresponding fields. These amplitude coefficients are found by satisfying the boundary conditions at $r = \rho_N$, which are equivalent to continuity of

$$\Phi^i(r)\big|_{r=\rho_N} + \Phi^r(r)|_{r=\rho_N} = \Phi^t(r)\big|_{r=\rho_N}, \tag{30}$$

and

$$\frac{\mathrm{d}}{\mathrm{d}r}\left[\Phi^i(r) + \Phi^r(r)\right]\Big|_{r=\rho_N} = \frac{\mathrm{d}\Phi^t(r)}{\mathrm{d}r}\Big|_{r=\rho_N}. \tag{31}$$

By solving the two equations for R and S in terms of A, we determine the power transmission coefficient given by Eq. (10) as

$$T = 1 - \left|\frac{R}{A}\right|^2, \tag{32}$$

which leads to the result (see Eq. (3) of Ref. [9])

$$T = \frac{4}{\pi^2}\frac{C_2}{X^2+Y^2}, \tag{33}$$

where, following the nomenclature of Ref. [9], the correct expressions for the coefficients X and Y are given by

$$\begin{aligned} X &= -A_1'A_2 + B_1'B_2 + A_1\left(C_1A_2 - C_2A_2'\right) - B_1\left(C_1B_2 - C_2B_2'\right), \\ Y &= A_1'B_2 + B_1'A_2 - B_1\left(C_1A_2 - C_2A_2'\right) - A_1\left(C_1B_2 - C_2B_2'\right), \end{aligned}$$

where

$$A_1 \equiv \mathrm{Ai}(\xi_1), \quad A_2 \equiv \mathrm{Ai}(\xi_2), \quad B_1 \equiv \mathrm{Bi}(\xi_1), \quad \text{and} \quad B_2 \equiv \mathrm{Bi}(\xi_2),$$

and prime denotes differentiation with respect to the arguments. Such a simplification is possible because the Wronskian of Airy functions dictates that $W\{\mathrm{Ai}(\xi), \mathrm{Bi}(\xi)\} = \pi^{-1}$, as stated in Ref. [23]. For the profile given in Eq. (13), $\xi_1 \equiv \xi_1(\rho_N)$ of Eq. (22) is evaluated by performing a numerical integration of Eq. (24), whereas $\xi_2 \equiv \xi_2(\rho_N)$ of Eq. (23) is readily calculated. Consequently

$$\xi_1 = \begin{cases} -\left[\dfrac{3}{2}\displaystyle\int_{\rho_N}^{r_{tp}} k_{r_1}(r)\,\mathrm{d}r\right]^{2/3}; & k_{r_1}^2 > 0, \\ +\left[\dfrac{3}{2}\displaystyle\int_{r_{tp}}^{\rho_N} |k_{r_1}(r)|\,\mathrm{d}r\right]^{2/3}; & k_{r_1}^2 < 0, \end{cases} \tag{34}$$

#10272 - $15.00 USD Received 11 January 2006; revised 6 February 2006; accepted 13 February 2006

and

$$\xi_2 = \begin{cases} -\left[\frac{3}{2}k\rho_N\left\{\left(n_{cl}^2-\tilde{\beta}^2-\tilde{l}^2\right)^{1/2}-\tilde{l}\arccos\left[\frac{\tilde{l}}{\left(n_{cl}^2-\tilde{\beta}^2\right)^{1/2}}\right]\right\}\right]^{2/3}; & k_{r_2}^2>0, \\ +\left[\frac{3}{2}k\rho_N\left\{\tilde{l}\ln\left[\frac{\tilde{l}+\left(\tilde{\beta}^2+\tilde{l}^2-n_{cl}^2\right)^{1/2}}{\left(n_{cl}^2-\tilde{\beta}^2\right)^{1/2}}\right]-\left(\tilde{\beta}^2+\tilde{l}^2-n_{cl}^2\right)^{1/2}\right\}\right]^{2/3}; & k_{r_2}^2<0, \end{cases} \tag{35}$$

being $k_{r_1}^2 \equiv k_{r_1}^2(\rho_N)$ and $k_{r_2}^2 \equiv k_{r_2}^2(\rho_N)$ given by Eqs. (24) and (25), respectively. The coefficients C_1 and C_2, which also depend on another four coefficients M_1, M_2, L_1 and L_2, are shown below (note that the last five coefficients given in Ref. [9] had to be corrected)

$$C_1 = (L_2-L_1)/M_1, \qquad C_2 = -M_2/M_1,$$

$$M_1 = \xi_1' = \frac{k_{r_1}}{(-\xi_1)^{1/2}}, \qquad M_2 = \xi_2' = \frac{-k_{r_2}}{(-\xi_2)^{1/2}},$$

$$L_1 = \frac{1}{4}\left(\frac{\xi_1'}{\xi_1}-\frac{2k_{r_1}'}{k_{r_1}}\right) = \frac{-k_{r_1}}{4(-\xi_1)^{3/2}}-\frac{k_{r_1}'}{2k_{r_1}}, \quad L_2 = \frac{1}{4}\left(\frac{\xi_2'}{\xi_2}-\frac{2k_{r_2}'}{k_{r_2}}\right) = \frac{k_{r_2}}{4(-\xi_2)^{3/2}}-\frac{k_{r_2}'}{2k_{r_2}},$$

being $\xi_1' \equiv [\mathrm{d}\xi_1(r)/\mathrm{d}r]|_{r=\rho_N}$, $\xi_2' \equiv [\mathrm{d}\xi_2(r)/\mathrm{d}r]|_{r=\rho_N}$, where $\xi_1(r)$ and $\xi_2(r)$ are given by Eqs. (22) and (23), respectively, and

$$k_{r_1}' \equiv \left.\frac{\mathrm{d}k_{r_1}(r)}{\mathrm{d}r}\right|_{r=\rho_N} = \begin{cases} \left.k\dfrac{\frac{\tilde{l}^2\rho_N^2}{r^3}+\frac{1}{2}\frac{\mathrm{d}n^2(r)}{\mathrm{d}r}}{\left[n^2(r)-\tilde{\beta}^2-\frac{\tilde{l}^2\rho_N^2}{r^2}\right]^{1/2}}\right|_{r=\rho_N} = k\dfrac{\tilde{l}^2/\rho_N+\delta/2}{\left(n_N^2-\tilde{\beta}^2-\tilde{l}^2\right)^{1/2}}; & k_{r_1}^2>0, \\ \left.\imath k\dfrac{-\frac{\tilde{l}^2\rho_N^2}{r^3}-\frac{1}{2}\frac{\mathrm{d}n^2(r)}{\mathrm{d}r}}{\left[\tilde{\beta}^2+\frac{\tilde{l}^2\rho_N^2}{r^2}-n^2(r)\right]^{1/2}}\right|_{r=\rho_N} = \imath k\dfrac{-\tilde{l}^2/\rho_N-\delta/2}{\left(\tilde{\beta}^2+\tilde{l}^2-n_N^2\right)^{1/2}}; & k_{r_1}^2<0, \end{cases} \tag{36}$$

$$k_{r_2}' \equiv \left.\frac{\mathrm{d}k_{r_2}(r)}{\mathrm{d}r}\right|_{r=\rho_N} = \begin{cases} \left.k\dfrac{\frac{\tilde{l}^2\rho_N^2}{r^3}}{\left(n_{cl}^2-\tilde{\beta}^2-\frac{\tilde{l}^2\rho_N^2}{r^2}\right)^{1/2}}\right|_{r=\rho_N} = k\dfrac{\tilde{l}^2/\rho_N}{\left(n_{cl}^2-\tilde{\beta}^2-\tilde{l}^2\right)^{1/2}}; & k_{r_2}^2>0, \\ \left.\imath k\dfrac{-\frac{\tilde{l}^2\rho_N^2}{r^3}}{\left(\tilde{\beta}^2+\frac{\tilde{l}^2\rho_N^2}{r^2}-n_{cl}^2\right)^{1/2}}\right|_{r=\rho_N} = \imath k\dfrac{-\tilde{l}^2/\rho_N}{\left(\tilde{\beta}^2+\tilde{l}^2-n_{cl}^2\right)^{1/2}}; & k_{r_2}^2<0. \end{cases} \tag{37}$$

For an MSI fibre of one layer the analytical continuation of $k_{r_1}(r)$ in Eq. (24) states that $r_{tp} \to \infty$ and, therefore, we have that $-\xi_1 \to \infty$. Under such circumstances, Eq. (33) reduces to

#10272 - $15.00 USD Received 11 January 2006; revised 6 February 2006; accepted 13 February 2006

the power transmission coefficient of an SI fibre [9]

$$T = \frac{4}{\pi}\frac{K_2}{Z^2+Y^2}, \tag{38}$$

where, fortunately, the expressions for the coefficients Z and Y were correctly given in Ref. [9]

$$Z = B_2 + K_1 A_2 - K_2 A_2',$$
$$Y = A_2 - K_1 B_2 + K_2 B_2',$$

even though the coefficient K_2 was incorrectly typed. The correct expressions for K_1 and K_2 are

$$K_1 = L_2/k_{r_1}, \qquad K_2 = -M_2/k_{r_1}.$$

As stated in Ref. [9], the same result could have been obtained if we invoked continuity of fields and their first derivative in Eqs. (30) and (31), after having replaced Φ^i and Φ^r of Eqs. (27) and (28) by

$$\Phi^i(r) = A\exp(\imath k_{r_1} r), \tag{39}$$
$$\Phi^r(r) = R\exp(-\imath k_{r_1} r). \tag{40}$$

Finally, it is important to bear in mind that the linearization of $n^2(r)$ in Eq. (13) leads to a different maximum value of $\tilde{l}$. It turns out to be that

$$\tilde{l}^2_{max}\left(\tilde{\beta}\right) = \frac{4}{27\delta^2\rho_N^2}\left[-\delta\rho_N - \left(\tilde{\beta}^2 - n_N^2\right)\right]^3, \tag{41}$$

which in some cases could be slightly lower than the value given by Eq. (7). In such a case, it is possible to use the expression given by Eq. (43), which is derived from the WKB approximation (see subsection 2.4 for further explanation). Since only weakly tunnelling rays are involved, the WKB expression will introduce a negligible error into the calculation of the power attenuation along the fibre.

2.4. WKB solutions of the scalar wave equation

It is possible to obtain separate expressions of the power transmission coefficient T for tunnelling and refracting rays within the local plane-wave approximation. These solutions, which are frequently referred to as the Wentzel-Kramer-Brillouin (WKB) asymptotic solutions of the scalar wave equation, lead to the simplest forms for T and also provide an excellent physical insight into the understanding of the phenomena involving both tunnelling and refracting rays [4].

Even though the WKB solutions for optical fibres can be generalized to include discontinuities in the refractive index profile [7], their applicability is only valid if $r_{rad} - r_{tp} \gg O(\lambda)$ [24]. In the limit where a tunnelling ray becomes a refracting one, i.e. if $r_{rad} \to \rho_N$, the power transmission coefficient obtained using the WKB approximation is inappropriate, and the expression derived by using the method of uniform approximation must be used instead (see Eq. (33) in subsection 2.3). All in all the WKB results are still a good enough approximation for weakly tunnelling rays, which have very small values of the power transmission coefficient [4].

For MSI fibres, the appropriate power transmission coefficient based on the WKB solutions has the form [7]

$$T = \prod_i \left|T_F^i\right| \exp\left[-2\int_{r_{tp}}^{r_{rad}} |k_r(r)|\,\mathrm{d}r\right], \tag{42}$$

#10272 - $15.00 USD Received 11 January 2006; revised 6 February 2006; accepted 13 February 2006

where T_F is the analytic continuation of the classical Fresnel transmission coefficient [25]. Each of the factors $\left|T_F^i\right|$ accounts for the ith discontinuity of the profile in the evanescent region and represents the power attenuation of a tunnelling ray due to the fraction of power reflected back towards the inside of the fibre. In the same way, the WKB integral in Eq. (42) represents the power reflected back over the continuous part of the refractive index profile [7].

Let us now particularize Eq. (42) to an MSI fibre of N layers. If a tunnelling ray has its outermost turning point at a certain layer $x \leqslant N$ according to Eq. (2), i.e. if $r_{tp} = \rho_x$, then

$$T_{tunnel} = \frac{4k_{r_x}^- \left|k_{r_x}^+\right|}{k^2\left(n_x^2 - n_{x+1}^2\right)} \prod_{i=x+1}^{N} \frac{4\left|k_{r_i}^-\right|\left|k_{r_i}^+\right|}{\left|k_{r_i}^-\right|^2 + \left|k_{r_i}^+\right|^2 + 2\left|k_{r_i}^-\right|\left|k_{r_i}^+\right|} \exp\left(\zeta_1 + \zeta_2\right), \tag{43}$$

where

$$k_{r_i}^- = k\left(n_i^2 - \tilde{\beta}^2 - \frac{\tilde{l}^2\rho_N^2}{\rho_i^2}\right)^{1/2}, \tag{44}$$

$$k_{r_i}^+ = k\left(n_{i+1}^2 - \tilde{\beta}^2 - \frac{\tilde{l}^2\rho_N^2}{\rho_i^2}\right)^{1/2}, \qquad (n_{N+1} = n_{cl}) \tag{45}$$

and

$$\zeta_1 = -2k\rho_N \sum_{i=x+1}^{N} \left(\left\{ \tilde{l} \ln \left[\frac{\frac{\tilde{l}\rho_N}{\rho_{i-1}} + \left(\tilde{\beta}^2 + \frac{\tilde{l}^2\rho_N^2}{\rho_{i-1}^2} - n_i^2\right)^{1/2}}{\left(n_i^2 - \tilde{\beta}^2\right)^{1/2}} \right] - \left[\tilde{l}^2 + \frac{\rho_{i-1}^2}{\rho_N^2}\left(\tilde{\beta}^2 - n_i^2\right) \right]^{1/2} \right\} - \left\{ \tilde{l} \ln \left[\frac{\frac{\tilde{l}\rho_N}{\rho_i} + \left(\tilde{\beta}^2 + \frac{\tilde{l}^2\rho_N^2}{\rho_i^2} - n_i^2\right)^{1/2}}{\left(n_i^2 - \tilde{\beta}^2\right)^{1/2}} \right] - \left[\tilde{l}^2 + \frac{\rho_i^2}{\rho_N^2}\left(\tilde{\beta}^2 - n_i^2\right) \right]^{1/2} \right\} \right), \tag{46}$$

$$\zeta_2 = -2k\rho_N \left\{ \tilde{l} \ln \left[\frac{\tilde{l} + \left(\tilde{\beta}^2 + \tilde{l}^2 - n_{cl}^2\right)^{1/2}}{\left(n_{cl}^2 - \tilde{\beta}^2\right)^{1/2}} \right] - \left(\tilde{\beta}^2 + \tilde{l}^2 - n_{cl}^2\right)^{1/2} \right\}. \tag{47}$$

Each of the factors inside the product of Eq. (43) is always within the interval

$$0 \leqslant \frac{4\left|k_{r_i}^-\right|\left|k_{r_i}^+\right|}{\left|k_{r_i}^-\right|^2 + \left|k_{r_i}^+\right|^2 + 2\left|k_{r_i}^-\right|\left|k_{r_i}^+\right|} \leqslant 1,$$

whereas the first factor (outside and on the left side of the product) does not satisfy the condition above. Instead, we have [22]

$$0 \leqslant \frac{4k_{r_x}^- \left|k_{r_x}^+\right|}{k^2\left(n_x^2 - n_{x+1}^2\right)} \leqslant 2,$$

since $\left(k_{r_x}^-\right)^2 > 0$ and $\left(k_{r_x}^+\right)^2 < 0$. It should be kept in mind that, in the boundary between tunnelling and refracting rays, this factor could be significant enough to lead to an overestimate WKB value of the power transmission coefficient in Eq. (43) and consequently invalidate the obtained result.

#10272 - $15.00 USD Received 11 January 2006; revised 6 February 2006; accepted 13 February 2006

Finally, the transmission coefficient for refracting rays reduces to the classical Fresnel transmission coefficient [21]

$$T_{refr} = \frac{4k_{r_N}^- k_{r_N}^+}{\left(k_{r_N}^- + k_{r_N}^+\right)^2} = \frac{4\left[\left(n_N^2 - \tilde{\beta}^2 - \tilde{l}^2\right)\left(n_{cl}^2 - \tilde{\beta}^2 - \tilde{l}^2\right)\right]^{1/2}}{\left(n_N^2 - \tilde{\beta}^2 - \tilde{l}^2\right) + \left(n_{cl}^2 - \tilde{\beta}^2 - \tilde{l}^2\right) + 2\left[\left(n_N^2 - \tilde{\beta}^2 - \tilde{l}^2\right)\left(n_{cl}^2 - \tilde{\beta}^2 - \tilde{l}^2\right)\right]^{1/2}}. \quad (48)$$

3. Results and discussion

3.1. Structural characteristics of the analysed fibres

In the calculations carried out we have chosen characteristics typical of poly-methyl-methacrylate PMMA-based polymer optical fibres (POF). Then we will be able to compare the results obtained for SI, clad-parabolic-profile GI and parabolic-profile MSI fibres with the results for two existing MSI-POFs. Nevertheless, any conclusion drawn from this analysis can be easily extrapolated to any kind of highly multimode optical fibre used as a transmission medium.

For SI and clad-parabolic-profile GI fibres, we have chosen the value 1.492 as the highest refractive index in the core and 1.402 as the refractive index of the cladding (n_{cl}), whereas the radius of the core of the fibre has been set to $\rho = 490\ \mu$m. We have already demonstrated that an MSI fibre of one layer is a limit case in which the power transmission coefficient reduces to that corresponding to an SI fibre (see Eq. (38) in subsection 2.3). The other limit case consists in an MSI fibre whose refractive index profile approximates to a clad-parabolic one of a GI fibre. Provided that the MSI fibre has a sufficiently high number of layers and by maintaining the width of each layer constant (i.e. $\rho_i - \rho_{i-1} = \text{constant}\ \forall i$), this second case can be achieved if we fit the refractive index of each layer to

$$n_{MSI,i} = n_{GI}(r)\Big|_{r=\rho_{i-1}} \qquad \forall i \qquad (\rho_0 = 0).$$

This enables us to test the validity of the theoretical expression by comparing the results obtained for a clad-parabolic-profile GI fibre with those for parabolic profile MSI fibres of an arbitrary number of layers.

The two MSI-POFs investigated in this paper are the Eska-Miu fibre from Mitsubishi [26] and the MSI-POF from TVER [1]. The physical dimensions of their layers are reproduced in Table 1, whereas Figs. 2(a) and 2(b) show their respective refractive index profiles measured with the aid of the inverse-near-field method [27, 28]. We have taken the value of 1.492 as the refractive index of the innermost layer (n_1), considering a value of 1.402 as the refractive index of the cladding (n_{cl}). The refractive indices of the remaining layers in between are adjusted according to the measured refractive index profiles relative to the extreme values n_1 and n_{cl}.

Table 1. Physical dimensions of the different layers (outer radii in μm).

	Layer 1	Layer 2	Layer 3	Layer 4
Eska-Miu	250	350	380	–
TVER	160	230	270	330

#10272 - $15.00 USD Received 11 January 2006; revised 6 February 2006; accepted 13 February 2006

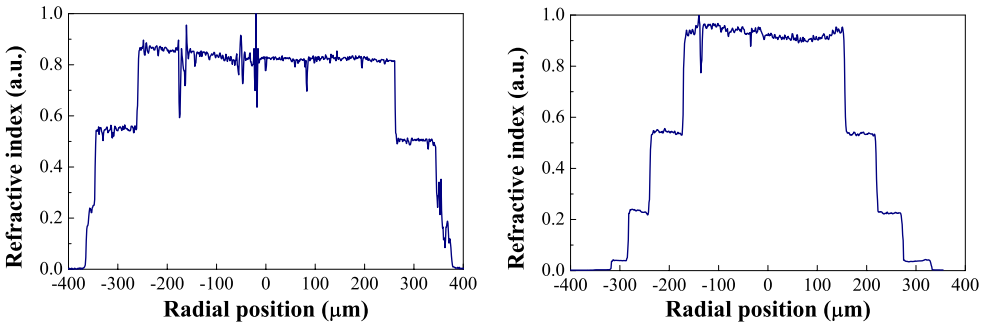

(a) Eska-Miu fibre. (b) TVER fibre.

Fig. 2. Refractive index profiles corresponding to the MSI-POFs used.

3.2. *Distribution of the power transmission coefficient for tunnelling and refracting rays on the $\tilde{\beta}^2$-$\tilde{l}^2$ plane*

The contour plots in Fig. 3 show the numerical results for the power transmission coefficient of Eq. (33) as a function of the square of the ray invariants $\tilde{\beta}$ and $\tilde{l}$ for the wavelength $\lambda = 650$ nm and for the different fibres considered in subsection 3.1.

The dashed dotted line superimposed on the $\tilde{\beta}^2$-$\tilde{l}^2$ plane shows the limit where a tunnelling ray becomes a refracting one. In the case of the clad-parabolic-profile GI fibre (see Fig. 3(b)), this boundary is restricted to the interval between ($\tilde{\beta}^2_{min}$, $n^2_{cl} - \tilde{\beta}^2_{min}$) and ($n^2_{cl}$, 0), where $\tilde{\beta}^2_{min}$ is a minimum value below which there are only refracting rays [29]. Conversely, in SI and MSI fibres this boundary extends along the whole $\tilde{\beta}^2$-$\tilde{l}^2$ plane, or more specifically, from (0, n^2_{cl}) to (n^2_{cl}, 0). The discontinuity of the refractive index profile in the core-cladding interface ensures this, even though the region of tunnelling rays is reduced as the jump in the discontinuity decreases. The limit case constitutes a parabolic-profile MSI fibre of $N \to \infty$ layers, in which the refractive index profile reduces to a continuous graded-index one.

It can be observed in Fig. 3(a) that tunnelling rays have great significance in SI fibres, since in most cases their power transmission coefficient is close to 0 and, therefore, they can propagate long distances before being completely attenuated. This suggests that tunnelling rays should be taken into account in geometric optics. As a consequence, it would be preferable the assignment of a simplified value of $T = 0$ to tunnelling rays to a rejection of them. In contrast, the set of Figs. 3(b) and 3(c) show that the region of tunnelling rays in both the clad-parabolic-profile GI fibre and the parabolic-profile MSI fibre of $N = 1\,000$ layers is quite small. Additionally, it is noticeable that the change of T in the transition region between tunnelling and refracting rays is very abrupt, whereas in the case of an SI fibre T changes gradually as tunnelling rays become refracting rays.

The cases corresponding to the Eska-Miu and TVER MSI-POFs, which share similar characteristics (the former has three layers, whereas the latter has four), deserve careful consideration. We can observe in Fig. 3(e) that the region of tunnelling rays in the TVER fibre is quite small and similar to that of a clad-parabolic-profile GI fibre, whereas the Eska-Miu exhibits a wider region of tunnelling rays, in accordance with Fig. 3(d) (their proportion to bound rays is also more significant). In order to be able to understand the reason for such a behaviour, we have to refer to their refractive index profiles (see Figs. 2(a) and 2(b)). Although the outermost layer of the Eska-Miu fibre is extremely thin, the great difference between the refractive indices of this layer and the cladding allows greater values of $\tilde{l}^2_{max}$ in Eq. (7) and, therefore, this leads to a much greater extension of the region of tunnelling rays than in the case of the TVER fibre,

#10272 - $15.00 USD Received 11 January 2006; revised 6 February 2006; accepted 13 February 2006

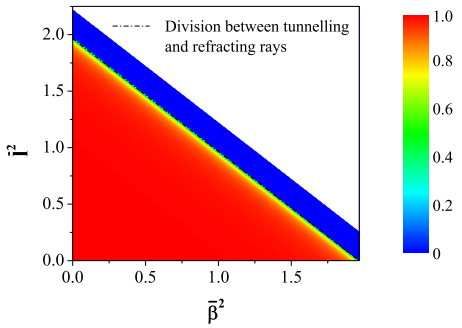

(a) SI fibre.

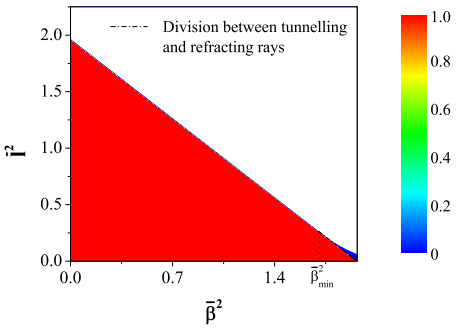

(b) Clad-parabolic-profile GI fibre.

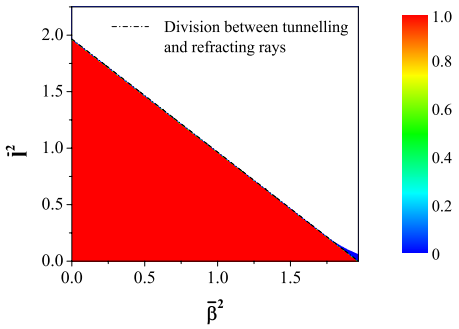

(c) Parabolic-profile MSI fibre ($N = 1\,000$).

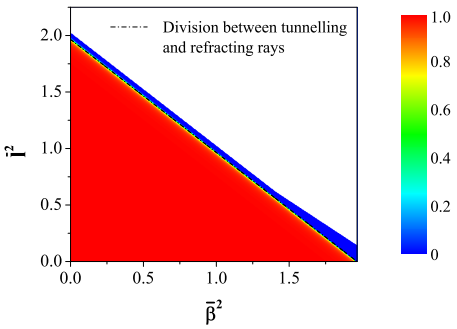

(d) Eska-Miu fibre.

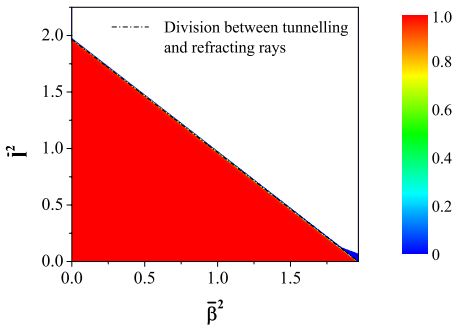

(e) TVER fibre.

Fig. 3. Contour plots of the power transmission coefficient T on the $\tilde{\beta}^2$-$\tilde{l}^2$ plane, calculated for both tunnelling and refracting rays and for the wavelength $\lambda = 650$ nm. The dashed dotted line shows the limit where a tunnelling ray becomes a refracting ray.

#10272 - $15.00 USD Received 11 January 2006; revised 6 February 2006; accepted 13 February 2006

where this difference is smaller.

3.3. *Investigation of the limit cases of MSI fibres*

Figure 4 shows graphs of the power transmission coefficient calculated using Eq. (33) with constant $\tilde{l} = 0.255$ for parabolic-profile MSI fibres of $N = 1$, 5, 10, 100, 1 000 and 10 000 layers, respectively. The vertical dashed dotted line superimposed on Fig. 4 shows again the limit where a tunnelling ray becomes a refracting ray, which occurs when $\tilde{\beta}^2 + \tilde{l}^2 = n_{cl}^2$, or more specifically, at $\tilde{\beta} = 1.3786$ for the constant value $\tilde{l} = 0.255$.

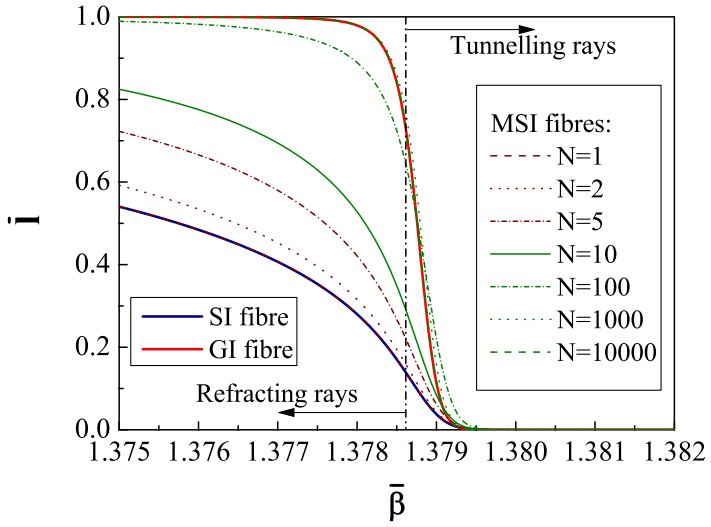

Fig. 4. Evolution of the power transmission coefficient T as a function of the number of layers N of an MSI fibre with constant $\tilde{l} = 0.255$. Results obtained for the wavelength $\lambda = 650$ nm. The blue and red solid curves denote the results for the SI and clad-parabolic-profile GI fibres, respectively. The dashed dotted vertical line shows the division between tunnelling and refracting rays, which occurs at $\tilde{\beta} = 1.3786$, when $\tilde{\beta}^2 + \tilde{l}^2 = n_{cl}^2$.

As could be expected, the power transmission coefficient for an MSI fibre of one layer is the same as that for an SI fibre. On the other hand, it is clearly noticeable that as the number of layers increases, the obtained results for the parabolic-profile MSI fibres approximate better to the result corresponding to a clad-parabolic-profile GI fibre. For instance, the power transmission coefficient calculated for a parabolic-profile MSI fibre of $N = 1\,000$ layers is very similar to that for a clad-parabolic-profile GI fibre, and in the limit case of $N = 10\,000$ layers, both results are virtually the same. In view of the results, we can safely conclude that our theoretical expression is valid and sufficiently accurate.

3.4. *Comparison between the uniform method and the WKB approximation*

Figure 5 allows us to compare the results obtained using the power transmission coefficient T derived from the uniform method with the results for T based on the WKB solutions of the scalar wave equation. The solid curves plot the power transmission coefficient of Eq. (33) as a function of $\tilde{\beta}$ with constant $\tilde{l} = 0.255$, whereas the dashed curves plot T corresponding to Eqs. (43) and (48). In addition, we have used different colours to identify the results obtained for the parabolic-profile MSI fibre of $N = 1\,000$ layers (blue curves) and both Eska-Miu (red curves) and TVER (green curves) MSI-POFs.

#10272 - $15.00 USD Received 11 January 2006; revised 6 February 2006; accepted 13 February 2006

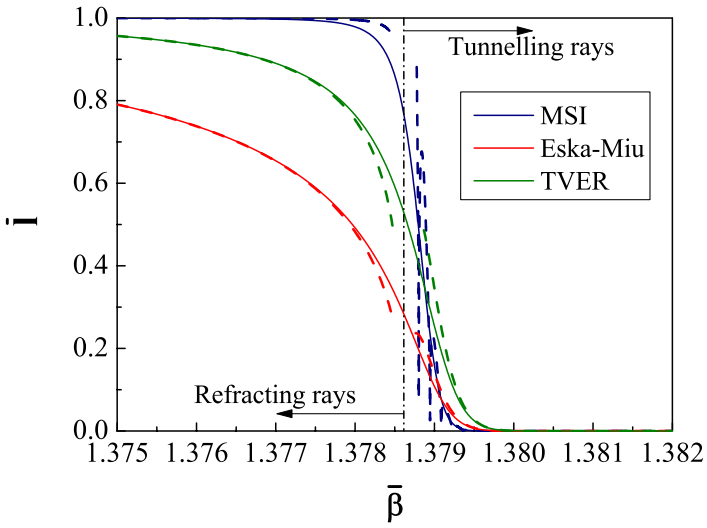

Fig. 5. Comparison between the uniform method and the WKB approximation. Plots of the power transmission coefficient T with constant $\tilde{l} = 0.255$ for the wavelength $\lambda = 650$ nm. Results obtained for the parabolic-profile MSI fibre of $N = 1\,000$ layers and both Eska-Miu and TVER MSI-POFs. Legend: T of Eq. (33): solid curves; T of Eqs. (43) and (48): dashed curves. The dashed dotted vertical line at $\tilde{\beta} = 1.3786$ corresponds to the limit $\tilde{\beta}^2 + \tilde{l}^2 = n_{cl}^2$. To the right of this limit value rays are tunnelling, whereas to the left they are refracting.

As anticipated in subsection 2.4, the extraordinary coincidence of dashed and solid curves on Fig. 5 indicates that the WKB representations are highly accurate for practically all tunnelling and refracting rays except for points located very close to the division between tunnelling and refracting rays. Within this transition region the WKB analysis is inappropriate and leads to an incorrect value of the power transmission coefficient [7, 8, 24]. Instead, Eq. (33) of the uniform method must be applied. It should be emphasized that this equation is not only valid for every domain of the set of leaky rays, but it also incorporates them into a single analytical expression, which is considerably advantageous for computational purposes [4, 9].

The jumps observed on the blue dashed curve corresponding to tunnelling rays in the parabolic-profile MSI fibre of $N = 1\,000$ layers are obtained as a result of the factors inside the product of Eq. (43), which account for the discontinuities of the profile in the evanescent region. It must be pointed out that as the number of layers of an MSI fibre increases indefinitely, the limit of the product of Eq. (43) reduces to the WKB integral of a GI fibre [7]. In contrast, the red and green dashed curves show no jumps at all because it turns out that in the Eska-Miu and the TVER MSI-POFs every tunnelling ray has its outermost turning point at the outermost layer, i.e. $r_{tp} = \rho_N$ for all tunnelling rays.

4. Conclusions

We have obtained a single theoretical expression that allows the calculation of the power transmission coefficient in MSI fibres. Such an expression will be of great benefit for computational purposes, since its implementation will lead to more elaborate and accurate results when performing computer simulations using the ray-tracing method. This theoretical expression has been derived by using the method of uniform approximation and relies on the linearization of the square of the core refractive index profile. In contrast to the WKB approximations, whose

#10272 - $15.00 USD Received 11 January 2006; revised 6 February 2006; accepted 13 February 2006

validity is restricted to specific domains of the set of leaky rays, this power transmission coefficient is valid for tunnelling and refracting rays, and for the transition between them. We have validated our theoretical model by carrying out several calculations of the power transmission coefficient for different types of MSI fibres and by comparing them with the results corresponding to SI and clad-parabolic GI fibres. The obtained results have also served us to find out that tunnelling rays can have an important effect on the power attenuation along an MSI fibre and that this effect depends strongly on the fibre refractive index profile.

Acknowledgments

This work was supported by the *Universidad del País Vasco–Euskal Herriko Unibertsitatea*, the *Gobierno Vasco–Eusko Jaurlaritza*, and the *Ministerio de Ciencia y Tecnología* under projects GIU05/03, UE05/A25, HEGATEK-05, SENSOFIB/SAIOTEK, and TIC2003-08361.

#10272 - $15.00 USD Received 11 January 2006; revised 6 February 2006; accepted 13 February 2006